Journal of Young Pharmacists, 2026; 18(3):709-719.
https://www.jyoungpharm.org

Original Article

Design, Synthesis and Molecular Dynamics Simulation of Novel Spiropyran Derivatives as Putative CDK6-Targeting Anticancer Agents for Breast Cancer Treatment

Sagar D. Magar[1,*], Shubham P. Mankar[1], Sanket K. Tambe[1], Amol S. Dighe[1], Nilima M. Wani[1], Mayur S. Bhosale[1], Rahul K. Godge[1], Dattaprasad N. Vikhe[2], Jagdish R. Kudnar[2]

[1]Department of Pharmaceutical Chemistry, Pravara Rural College of Pharmacy, Pravaranagar, Maharashtra, INDIA.
[2]Department of Pharmacognosy, Pravara Rural College of Pharmacy, Pravaranagar, Maharashtra, INDIA.

ABSTRACT

Background: Breast cancer treatment with current dual CDK4/6 inhibitors is limited by hematological toxicity and acquired drug resistance. CDK6 is overexpressed in specific breast cancer subtypes and represents a validated molecular target for the development of new anticancer agents. This study aimed to design, synthesize, and evaluate novel spiropyran derivatives as putative CDK6-targeting anticancer agents for breast cancer treatment. **Materials and Methods:** Eight spiropyran derivatives (S1-S8) were designed and evaluated through drug-likeness assessment, ADME/toxicity prediction using ForceADME and Geintox-II, and molecular docking against CDK6 (PDB ID: 5L2I) using GeinDock Suite v2.3.1.0. Selected complexes were subjected to 100 ns molecular dynamics simulations with MM-GBSA binding free energy calculations using Desmond/Prime. Compounds were synthesized via multi-step condensation reactions, characterized by IR, ^{1}H NMR, ^{13}C NMR, and MS, and selected derivatives evaluated for *in vitro* cytotoxicity against MCF-7 breast cancer cells using MTT assay (n=3, triplicates). **Results:** Among the eight derivatives, compound S5 showed the highest predicted CDK6 binding affinity (-9.8 kcal/mol), marginally higher than palbociclib (-9.4 kcal/mol), with dual hydrogen bonds to GLY20 and TYR24. Molecular dynamics simulations indicated a binding free energy for S5 (ΔG^{bcT} = -131.12±7.76 kcal/mol) comparable to palbociclib (-127.66±5.26 kcal/mol). *In vitro* cytotoxicity revealed an IC_{50} of 15.58±1.24 µM for S5, comparable to palbociclib (17.33±1.38 µM) in MCF-7 cells. **Conclusion:** The observed agreement between computational predictions and *in vitro* cytotoxicity for the three experimentally evaluated compounds supports the spiropyran scaffold as a candidate framework warranting further investigation. Spiropyran derivative S5 represents an early-stage lead with distinct CDK6 binding interactions, requiring confirmatory kinase inhibition assays, selectivity profiling, and *in vivo* efficacy studies before its therapeutic potential can be established.

Keywords: Breast cancer, CDK6 inhibitors, Cytotoxicity, MM-GBSA, Molecular dynamics simulation, Spiropyran derivatives.

Correspondence:
Dr. Sagar Magar
Department of Pharmaceutical Chemistry, Pravara Rural College of Pharmacy, Pravaranagar, Maharashtra, INDIA.
Email: sagarmagar2010@gmail.com
ORCID:0000-0001-8467-849X

Received: 22-06-2026;
Revised: 12-08-2026;
Accepted: 01-09-2026.

INTRODUCTION

Breast cancer remains one of the foremost health challenges worldwide, with hormone receptor-positive subtypes accounting for the majority of diagnosed cases (Schettini *et al.*, 2020). The development of cyclin-dependent kinase 4 and 6 (CDK4/6) inhibitors has fundamentally altered the therapeutic landscape for these patients, offering remarkable improvements in progression-free survival when combined with endocrine therapy (Piezzo *et al.*, 2020; Zhou *et al.*, 2023). However, the clinical success of current CDK4/6 inhibitors has been tempered by persistent challenges, including acquired drug resistance (Shanabag *et al.*, 2025), dose-limiting toxicities that necessitate treatment modifications (Loibl and Furlanetto, 2022; Stanciu *et al.*, 2023), and the absence of true isoform selectivity between CDK4 and CDK6 (Watt and Goel, 2022). These limitations underscore the urgent need for next-generation inhibitors with improved selectivity and the ability to circumvent resistance mechanisms.

The molecular basis for CDK4/6 inhibitor activity centres on preventing Retinoblastoma (Rb) protein phosphorylation, thereby blocking cell cycle progression from G1 to S phase (Topacio *et al.*, 2019; Kim *et al.*, 2022). While palbociclib, ribociclib, and abemaciclib have demonstrated clinical efficacy

OPEN ACCESS
Manuscript TECHNOMEDIA

DOI: 10.5530/jyp.20260236

Copyright Information :
Copyright Author (s) 2026 Distributed under Creative Commons CC-BY 4.0

Publishing Partner : Manuscript Technomedia. [www.mstechnomedia.com]

in the metastatic setting, their combined inhibition of CDK4 and CDK6 contributes to dose-limiting hematological adverse events, primarily neutropenia (Sherr *et al.*, 2016; Scheicher *et al.*, 2015). The rationale for targeting CDK6 in breast cancer derives not from an expectation of an inherent safety advantage, since CDK6 activity in normal haematopoietic cells is itself a recognised contributor to this toxicity, but from the documented overexpression and amplification of CDK6 in specific aggressive subtypes, in which tumour cells display marked dependency on CDK6-driven cell cycle progression (Tadesse *et al.*, 2015). Identifying structurally distinct scaffolds that engage CDK6 therefore remains of interest, with the recognition that any safety differentiation relative to approved CDK4/6 inhibitors would require direct experimental verification.

Spiropyran derivatives represent an underexplored scaffold in kinase inhibitor development. These photochromic compounds possess a unique structural architecture characterised by a spiro junction connecting indoline and chromene moieties, creating a three-dimensional molecular framework amenable to pharmacological optimisation (Fagan *et al.*, 2021). Despite extensive investigation in materials science and sensor applications, their potential as kinase inhibitors has not been systematically explored (Ali *et al.*, 2020). The structural diversity accessible through synthetic modification of the spiropyran core makes this scaffold particularly attractive for structure-activity relationship studies aimed at achieving kinase selectivity (Keyvan Rad *et al.*, 2022).

Computational modelling studies suggest that appropriately substituted spiropyran derivatives can exploit subtle differences in the ATP-binding site architecture between CDK4 and CDK6 (Durrant and McCammon, 2011; Li *et al.*, 2023), potentially exhibiting computationally predicted differential binding toward CDK6 that would require direct comparative kinase assays to be established as true selectivity. This study describes the design, synthesis, and biological evaluation of novel spiropyran derivatives (S1-S8) as putative CDK6-targeting anticancer agents for breast cancer treatment. We hypothesised that structural modifications of the spiropyran core would enhance CDK6 binding affinity while maintaining favourable drug-like properties. The novelty lies in employing photoswitchable spiropyran scaffolds for CDK engagement, validated through comprehensive molecular dynamics simulations and MM-GBSA calculations.

MATERIALS AND METHODS

Materials

2,3,3-Trimethyl-3H-indole (98%) was procured from Sciquaint Chemicals (Pune, India). Substituted 2-hydroxybenzaldehydes (99%) were obtained from HiMedia Laboratories (Mumbai, India). Anhydrous ethanol (99.5%, HPLC grade) and piperidine (99%) were sourced from Neeta Chemicals (Pune, India). MTT [3-(4,5-dimethylthiazol-2-yl)-2,5-diphenyltetrazolium bromide] (98%) and DMSO (99.9%) were purchased from Research Lab Fine Chem Industries (Pune, India). Palbociclib reference standard (99%, MW 447.54 g/mol) was obtained from Sciquaint Innovations Pvt. Ltd., (Pune, India). MCF-7 breast cancer cell line was procured from the National Centre for Cell Science (NCCS, Pune, India). DMEM culture medium, Fetal Bovine Serum (FBS), and phosphate-buffered saline (PBS, pH 7.4) were obtained from SRL Diagnostics (Mumbai, India) and Central Drug House (New Delhi, India), respectively. All other reagents were of analytical grade.

Experimental Design

The study followed a rational drug design approach: eight spiropyran derivatives (S1-S8) were designed based on computational docking against CDK6 (PDB ID: 5L2I), synthesised and characterised spectroscopically, then evaluated computationally (ADME, toxicity, molecular dynamics) and experimentally (MTT cytotoxicity assay). Compounds with docking scores >-9.0 kcal/mol and favourable predicted ADME profiles were prioritised for *in vitro* evaluation. Sample size of eight derivatives was determined based on systematic variation of the nucleophilic substituent at the N-1 position of the spiropyran core to establish structure-activity relationships.

Drug-Likeness, ADME, and Toxicity Prediction

Pharmacokinetic properties and drug-likeness were evaluated using ForceADME (Geinforce Technology Pvt. Ltd., Pune, India; https://geinforce.com/force-adme/). SMILES notations generated in ChemDraw were submitted for Lipinski's Rule of Five assessment, oral bioavailability prediction, intestinal absorption, Blood-Brain Barrier (BBB) penetration, P-glycoprotein substrate recognition, cytochrome P450 inhibition profiles, and synthetic accessibility scores. Toxicity profiles were assessed using Geintox-II (Geinforce Technology Pvt. Ltd., Pune, India; https://geinforce.com), a computational toxicology platform employing machine learning algorithms trained on curated toxicological databases (Bhandari *et al.*, 2026). Endpoints evaluated included acute oral toxicity (LD_{50}, toxicity class), hepatotoxicity, carcinogenicity, mutagenicity, immunotoxicity, cytotoxicity, respiratory toxicity, and blood-brain barrier penetration.

Molecular Docking

Molecular docking was performed using GeinDock Suite v2.3.1.0 (Geinforce Technology Pvt. Ltd., Pune, India), with results validated against AutoDock Vina (correlation coefficient r^2=0.89). The CDK6 crystal structure (PDB ID: 5L2I) was prepared by removal of water molecules and heteroatoms, followed by addition of polar hydrogens and Gasteiger charges. Spiropyran derivatives were energy-minimised using the MMFF94 force field for 2500 steps. The docking grid was centred at x: -13.7515, y: 28.1005, z: 9.7195 Å, with box dimensions of 25 × 25 × 25 $Å^3$. Protocol validation was confirmed by redocking

the co-crystallised palbociclib, achieving RMSD<2.0 Å. Three-dimensional interactions and 2D ligand-protein diagrams were generated using BIOVIA Discovery Studio Visualizer v4.5.

Molecular Dynamics Simulation and MM-GBSA Analysis

Molecular Dynamics (MD) simulations of palbociclib-CDK6 and S5-CDK6 complexes were conducted using Desmond v2020.1 (Schrödinger, LLC) with the OPLS-2005 force field and TIP3P water model in a cubic periodic boundary box (Bowers *et al.*, 2006; Shivakumar *et al.*, 2010). The system was neutralised with sodium ions and supplemented with 0.15 M NaCl. Energy minimisation was followed by 10 ns NVT and 12 ns NPT equilibration phases using the Nosé-Hoover thermostat at 300 K and 1 bar (Ivanova *et al.*, 2018). Production simulations were run for 100 ns; stability was monitored via RMSD, RMSF, Radius of gyration (Rg), hydrogen bonding patterns, and Solvent Accessible Surface Area (SASA). The 100 ns duration was justified based on observed RMSD convergence of both complexes by 20 ns, with stable plateau values maintained throughout the production phase. Binding free energies were calculated using the MM-GBSA method via the Prime MM-GBSA module (Dasmahapatra *et al.*, 2022), processing 500 final trajectory frames using thermal_mmgbsa.py (Forouzesh and Mishra, 2021).

Synthesis of Spiropyran Derivatives (S1-S8)

The spiropyran derivatives were synthesised via a multi-step route. 2,3,3-Trimethyl-3H-indole (Sa, 1.0 mmol) was treated with 2-chloroacetyl chloride (1.2 mmol) in anhydrous DMF (5 mL) at 0°C for 2 hr to afford compound Sb (Mandal *et al.*, 2022). Compound Sb was treated with triethylamine (1.5 mmol) in anhydrous DCM (10 mL) at room temperature for 1 hr to generate compound Sc. The key spiropyran intermediate (Sd) was synthesised by reacting Sc (1.0 mmol) with 2-hydroxy-5-nitrobenzaldehyde (1.0 mmol) in anhydrous ethanol (15 mL) under reflux at 78°C for 4-6 hr. Final derivatives S1-S8 were obtained by refluxing Sd (1.0 mmol) with appropriate nucleophiles in anhydrous DCM (10 mL) containing pyridine (0.3 mL) at 40-45°C for 8-12 hr (Hughes-Whiffing and Perry, 2023). The synthesis scheme and proposed mechanism are illustrated in Figures 1 and 2, respectively. All compounds were characterised by IR, ^{1}H NMR (400 MHz), ^{13}C NMR (100 MHz, where applicable), ESI-MS, and elemental analysis (C, H, N).

In vitro Cytotoxicity Assay

Antiproliferative activity of compounds S2, S5, and S7, selected based on docking scores >-9.0 kcal/mol and favourable predicted ADME profiles, along with palbociclib, was evaluated against MCF-7 breast cancer cells using the MTT assay (Ramazi *et al.*, 2023). MCF-7 cells (1×10^4 cells/well) were seeded in 96-well plates in DMEM supplemented with 10% FBS and incubated at 37°C in 5% CO_2 for 24 hr (Razak *et al.*, 2019). Cells were treated with concentrations ranging from 1.56 to 100 µM (two-fold serial dilutions) for 72 hr. MTT solution (5 mg/mL, 20 µL/well) was added and incubated for 4 hr; formazan crystals were dissolved in 100 µL DMSO and absorbance measured at 570 nm (reference: 630 nm) using a microplate reader (BioTek, USA) (Ghasemi *et al.*, 2021). Each experiment comprised three independent biological replicates on separate days, each containing technical triplicates (n=3, expressed as Mean ± SD). IC_{50} values were determined by non-linear regression analysis using GraphPad Prism v9.0.

Statistical Analysis

Cytotoxicity data are expressed as Mean ± SD (n=3 independent experiments). IC_{50} values with 95% Confidence Intervals (CI) were derived from non-linear regression (GraphPad Prism v9.0). Statistical comparisons between compound IC_{50} values and palbociclib were performed using one-way Analysis of Variance (ANOVA) followed by Dunnett's post-hoc test. A p-value<0.05 was considered statistically significant. MM-GBSA binding free energy values are reported as Mean ± SD across 500 trajectory frames.

RESULTS

Drug-Likeness, ADME, and Toxicity Assessment

Drug-likeness and pharmacokinetic profiles of spiropyran derivatives S1-S8 are presented in Table 1. Compound S1 exhibited one violation of Lipinski's Rule of Five (MlogP=5.36), indicating increased lipophilicity relative to palbociclib (LogP=2.74) (Lipinski, 2004). Hydrogen bond acceptor counts (5-7) and donor counts (0-1) for all derivatives fell within acceptable ranges. Total Polar Surface Area (TPSA) values for compounds S3-S7 (98.98-127.85 Å²) exceeded the optimal range (60-90 Å²), which may limit membrane permeability (Ertl *et al.*, 2000), while S1, S2, S6, and S8 showed more favourable TPSA values (81.91-107.93 Å²), comparable to palbociclib (105.04 Å²). All compounds showed low predicted gastrointestinal absorption and were predicted to penetrate the blood-brain barrier (Table 1), a property warranting *in vivo* confirmation and consideration of potential central nervous system exposure. Compounds S5 and S7 were identified as P-glycoprotein substrates, similar to palbociclib, potentially affecting cellular accumulation. Toxicity assessment via Geintox-II (Table 2) classified all compounds as Toxicity Class 4 (prediction accuracy 85%). Compounds S3, S4 and S6 showed LD_{50} values (1151.7-1267.4 mg/kg) marginally lower than palbociclib (1382.5 mg/kg), with all derivatives classified within Toxicity Class 4. All spiropyran derivatives showed active predictions for hepatotoxicity, carcinogenicity, and respiratory toxicity, warranting careful genotoxicity evaluation in preclinical studies (Banerjee *et al.*, 2024). The low gastrointestinal absorption observed for all compounds except S8 represents a limitation that requires formulation strategies, such as nanoparticle-based or prodrug approaches, for oral delivery optimisation (Adon *et al.*, 2021).

Molecular Docking Results

Molecular docking against CDK6 (PDB ID: 5L2I) yielded binding energies ranging from -7.6 to -9.8 kcal/mol (Table 3). Compound S5 demonstrated the highest binding affinity (-9.8 kcal/mol), marginally higher than palbociclib (-9.4 kcal/mol), attributed to dual hydrogen bonding interactions with GLY20 (3.72 Å) and TYR24 (3.65 Å) and a long-range electrostatic association with LYS43 (4.91 Å) (Martin *et al.*, 2017). Compounds S2 and S7 also exhibited strong binding energies (-9.1 and -9.0 kcal/mol, respectively), forming critical hydrogen bonds with TYR24 and electrostatic interactions with ASP163 (Rana *et al.*, 2019; Susanti *et al.*, 2021). Compounds S3 and S4 relied primarily on hydrophobic and van der Waals forces (-8.2 kcal/mol each) without direct hydrogen bonding. In contrast, palbociclib primarily engages VAL101 (2.13 Å) and GLU99 (3.77 Å) through hydrogen bonds, indicating binding motifs for the spiropyran derivatives that are distinct from those of palbociclib (Wells *et al.*, 2020; Wander *et al.*, 2022). Molecular docking interaction images for S5, S2, and palbociclib are presented in Figure 3.

Molecular Dynamics Simulation and MM-GBSA Analysis

RMSD analysis (Figure 4A) revealed that the palbociclib-CDK6 complex maintained values averaging 1.78±0.32 Å after equilibration (20-100 ns), while S5-CDK6 showed slightly higher flexibility (2.05±0.48 Å), with fluctuations remaining within acceptable limits for stable protein-ligand complexes (<3 Å) (Farhadi *et al.*, 2025). Both complexes exhibited similar RMSF fluctuation patterns (Figure 4B); the palbociclib complex showed marginally higher fluctuations (average 1.11 Å) around residues 37-38 and 215 (flexible loop regions), while S5-CDK6 exhibited slightly lower RMSF values (average 1.0 Å). Radius of gyration analysis (Figure 4C) indicated maintained structural integrity for both complexes, with the S5-CDK6 complex showing a slightly more compact structure (Rg: 4.24-5.02 Å vs 5.0-5.66 Å for palbociclib), suggestive of stronger stabilising intramolecular interactions (Sarac *et al.*, 2025). Hydrogen bond formation (Figure 4D) was consistently higher for palbociclib-CDK6 (169-232 contacts) compared to S5-CDK6 (161-225 contacts). MM-GBSA binding free energy analysis (Table 4) indicated a marginally more favourable predicted binding free energy for the S5-CDK6 complex (ΔG^{bcT}=-131.12±7.76 kcal/mol) relative to palbociclib-CDK6 (-127.66±5.26 kcal/mol); given the overlapping standard deviations, the two complexes are best regarded as comparable, with the difference attributable primarily to enhanced lipophilic interactions (ΔG^{bcT}_Lipo: -28.55 vs -26.58 kcal/mol) (Dasmahapatra *et al.*, 2022).

In vitro Cytotoxicity

In vitro cytotoxicity evaluation against MCF-7 breast cancer cells demonstrated promising antiproliferative activity for the spiropyran derivatives. As shown in Figure 4E, compound S5 was the most active among the tested compounds, with an IC_{50} of 15.58±1.24 µM, which was comparable to palbociclib (IC_{50}=17.33±1.38 µM) (p>0.05, one-way ANOVA with Dunnett's test). Compound S2 showed moderate activity (IC_{50}=21.76±1.79 µM), while compound S7 (IC_{50}=24.18±2.03 µM) demonstrated lower potency, consistent with its docking score (-9.0 kcal/mol). High correlation coefficients (R^2>0.99) for all compounds confirmed robust dose-response relationships (Ji *et al.*, 2020). These results are consistent with the molecular docking rankings, with S5's highest predicted binding affinity (-9.8 kcal/mol) corresponding to the lowest IC_{50} value. The IC_{50} values observed in the micromolar range are consistent with early-stage lead identification and are commonly reported for structurally novel scaffolds before SAR-guided potency optimisation (Bora *et al.*, 2021; Manzoor *et al.*, 2025). Morphological analysis of MCF-7 cells revealed characteristic changes, including cell shrinkage, membrane blebbing, detachment, and debris formation, following treatment with S5 and palbociclib at their respective

Table 1: Lipinski's Rule of Five and ADME Parameters for Spiropyran Derivatives S1-S8 and Palbociclib.

Compound	MLogP	MW (g/mol)	HBA	HBD	Violations	TPSA (Å²)	GI Abs.	BBB Pen.
S1	5.36	442.47	5	0	1	81.91	Low	Yes
S2	3.89	441.49	5	1	0	84.71	Low	Yes
S3	1.58	422.44	6	0	0	98.98	Low	Yes
S4	1.48	408.41	6	0	0	98.98	Low	Yes
S5	1.08	470.48	7	1	0	114.14	Low	Yes
S6	3.22	457.49	6	1	0	107.93	Low	Yes
S7	0.41	486.48	7	1	0	127.85	Low	Yes
S8	3.50	428.44	5	0	0	84.59	High	Yes
Palbociclib	2.74	447.54	9	2	0	105.04	Low	Yes

HBA: Hydrogen bond acceptors; **HBD:** Hydrogen bond donors; **TPSA:** Total polar surface area; **GI Abs.:** Gastrointestinal absorption; **BBB Pen.:** Blood-brain barrier penetration. Data obtained using ForceADME (Geinforce Technology Pvt. Ltd., Pune, India).

Table 2: Toxicity Analysis of Spiropyran Derivatives S1-S8 and Palbociclib (Geintox-II).

Compound	LD_{50} (mg/kg)	Tox. Class	Hepatotox.	Carcinogen.	Mutagenicity	BBB Penetration	Cytotox.
Palbociclib	1382.5	4	I (40%)	I (54%)	A (73%)	A (92%)	I (57%)
S1	626.4	4	A (99%)	A (99%)	A (99%)	A (99%)	A (71.5%)
S2	490.4	4	A (99%)	A (99%)	A (99%)	A (99%)	A (71.9%)
S3	1238.6	4	A (87.5%)	A (99%)	A (99%)	A (99%)	A (74%)
S4	1267.4	4	A (81.1%)	A (97.4%)	A (97.4%)	A (97.4%)	I (68%)
S5	571.2	4	A (98.6%)	A (98.6%)	A (98.6%)	A (84.6%)	A (73.2%)
S6	1151.7	4	A (97.4%)	A (97.4%)	A (97.4%)	A (97.4%)	A (75.7%)
S7	556.4	4	A (99%)	A (99%)	A (99%)	A (85.1%)	I (68.5%)
S8	500	4	A (54%)	A (59%)	A (83%)	A (69%)	A (56%)

A = Active; I = Inactive; Tox. Class: Toxicity Class (Geintox-II prediction accuracy 85% for all compounds); BBB Penetration: predicted blood-brain barrier penetration (Active denotes predicted permeant); Hepatotox.: Hepatotoxicity; Carcinogen.: Carcinogenicity; Cytotox.: Cytotoxicity. Statistical prediction accuracy (%) shown in parentheses.

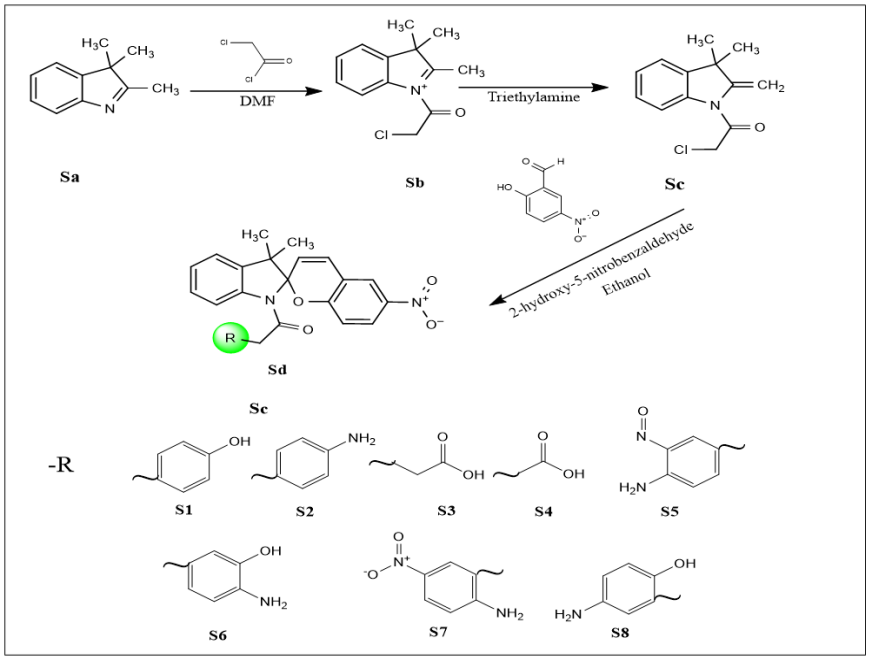


Figure 1: Synthesis scheme for spiropyran derivatives S1-S8. Reaction conditions: (i) 2-chloroacetyl chloride, DMF, 0°C, 2 hr; (ii) Et_3N, DCM, RT, 1 hr; (iii) 2-hydroxy-5-nitrobenzaldehyde, EtOH, reflux, 4-6 hr; (iv) appropriate nucleophile, pyridine, DCM, 40-45°C, 8-12 hr.

IC_{50} concentrations, consistent with CDK-inhibitor-induced cell-cycle arrest (Watt and Goel, 2022; Shanabag *et al.*, 2025).

DISCUSSION

The present study reports the design, synthesis, and evaluation of novel spiropyran derivatives as putative CDK6-targeting anticancer agents for breast cancer treatment. Compound S5 emerged as the lead candidate, demonstrating the highest predicted CDK6 docking affinity (-9.8 kcal/mol) in the series, marginally exceeding the approved CDK4/6 inhibitor palbociclib (-9.4 kcal/mol). These findings are consistent with published computational studies identifying dual hydrogen bond formation with the CDK6 hinge region as a key determinant of binding affinity; specifically, the GLY20 and TYR24 interactions observed for S5 are analogous to the interaction patterns reported for potent CDK6-binding compounds in recent structure-based drug design investigations (Martin *et al.*, 2017; Luo *et al.*, 2021; Debnath *et al.*, 2025). A long-range electrostatic association with LYS43 and extensive hydrophobic engagement of LEU152, PHE98, and ALA41 further distinguish S5 from the reference compound, which relies predominantly on VAL101 and GLU99 hydrogen bonds. These distinct binding motifs may be of pharmacological interest, since resistance mutations have been reported at conventional hinge-region interaction sites in patients treated with CDK4/6 inhibitors (Shanabag *et al.*, 2025); as resistance mechanisms were not investigated in the present

Table 3: Binding Energies and Molecular Interactions of Spiropyran Derivatives S1-S8 and Palbociclib with CDK6 (PDB ID: 5L2I).

Compound	Binding Energy (kcal/mol)	Hydrogen Bonds (Residue, Dist. Å)	Electrostatic Interactions (Residue, Dist. Å)	Key Hydrophobic Residues
S1	-7.6	LYS29 (3.35)	ASP104 (3.84)	ILE19, LEU152, HIS100, ALA41
S2	-9.1	TYR24 (3.24)	ASP163 (4.46)	ILE19, LEU152, PHE98, VAL27, ALA41, VAL77, VAL101, LYS43
S3	-8.2	None	ASP163 (4.33)	ILE19, LEU152, VAL27, ALA41, ALA162, VAL77, PHE98, VAL101, LYS43
S4	-8.2	None	None	ILE19, LEU152, VAL27, ALA41, ALA162, VAL77, PHE98, VAL101, LYS43
S5	-9.8	GLY20 (3.72), TYR24 (3.65)	LYS43 (4.91)	LEU152, VAL27, ALA41, ALA162, VAL77, PHE98, ILE19
S6	-8.1	TYR24 (3.30)	ASP163 (4.34)	ILE19, LEU152, VAL27, ALA41, ALA162, VAL77, PHE98, VAL101
S7	-9.0	TYR24 (3.23)	ASP163 (4.25)	ILE19, LEU152, PHE98, HIS100, VAL27, ALA41, VAL77, ALA162, VAL101
S8	-8.8	TYR24 (3.17)	ASP163 (4.40)	ILE19, LEU152, HIS100, VAL27, ALA41, ALA162, VAL77, PHE98, VAL101
Palbociclib	-9.4	VAL101 (2.13), GLU99 (3.77)	None	ILE19, VAL27, LEU152, ALA41, PHE98

GeinDock Suite v2.3.1.0 (Geinforce Technology Pvt. Ltd., Pune, India). Protocol validated by redocking co-crystallised palbociclib (RMSD < 2.0 Å). Binding energies validated against AutoDock Vina ($r^2 = 0.89$).

Table 4: MM-GBSA Binding Free Energy Components for Palbociclib-CDK6 and S5-CDK6 Complexes (Mean ± SD, *n*=500 trajectory frames).

Energy Component (kcal/mol)	Palbociclib-CDK6 Mean ± SD	S5-CDK6 Mean ± SD
ΔG^{beT} (Total)	-127.66±5.26	-131.12±7.76
ΔG^{beT} Coulomb	20.59±12.28	20.43±18.56
ΔG^{beT} Covalent	5.88±2.56	3.66±1.68
ΔG^{beT} H-bond	-5.71±0.99	-5.78±1.15
ΔG^{beT} Lipo	-26.58±1.41	-28.55±2.53
ΔG^{beT} Packing	-1.74±0.37	-1.68±0.92
ΔG^{beT} SolvGB	-20.05±12.14	-22.90±15.94
ΔG^{beT} vdW	-99.99±3.18	-96.34±3.08

MM-GBSA calculations performed using Prime MM-GBSA module (Schrödinger, LLC) processing 500 final trajectory frames. Lipo: Lipophilic; SolvGB: Solvation (Generalised Born); vdW: van der Waals. Relative comparisons between complexes are valid; absolute values may be overestimated due to implicit solvent approximation.

study, this remains a hypothesis requiring dedicated experimental validation.

Molecular dynamics simulations provided dynamic validation extending beyond static docking poses. Although S5 exhibited slightly higher RMSD flexibility (2.05±0.48 Å vs 1.78±0.32 Å for palbociclib), these values remained well within the threshold for stable protein-ligand complexes (<3 Å), consistent with productive binding (Farhadi *et al.*, 2025; Grewal *et al.*, 2025). The more compact radius of gyration observed for S5-CDK6 relative to palbociclib-CDK6 suggests stronger stabilising intramolecular interactions following ligand binding. MM-GBSA analysis indicated a more favourable predicted binding free energy for S5, driven primarily by enhanced lipophilic and van der Waals interactions (ΔG_Lipo:-28.55 vs -26.58 kcal/mol), consistent with the nitrosoaniline moiety of S5 making deeper contacts within the hydrophobic subpocket of the CDK6 ATP-binding site (Dasmahapatra *et al.*, 2022). Notably, the net Coulombic component of the decomposition was positive for both complexes (S5:+20.43±18.56 kcal/mol; palbociclib:+20.59±12.28 kcal/mol), reflecting an unfavourable electrostatic desolvation contribution;

binding was therefore governed by lipophilic and van der Waals terms rather than by net electrostatics, and the LYS43 contact observed in docking represents a long-range association that does not translate into a net favourable Coulombic contribution. The convergence of RMSD values by 20 ns and their stability for the remaining 80 ns justified the 100 ns simulation duration as sufficient to capture the equilibrium binding behaviour of both complexes.

The *in vitro* cytotoxicity results showed qualitative agreement with the computational rankings. S5 exhibited an IC_{50} of 15.58±1.24 µM against MCF-7 cells, statistically comparable to palbociclib (17.33±1.38 µM; $p>0.05$). The ordering of docking scores broadly tracked the observed cytotoxicity; however, no formal quantitative structure-activity relationship was derived, as a statistical correlation between binding free energies and biological activity across the series was not established, and any such relationship would require evaluation of a larger compound set. The micromolar IC_{50} values observed are characteristic of early-stage lead identification for structurally novel scaffolds and are in line with IC_{50} values reported for structurally related spiropyran and spiro-heterocyclic compounds evaluated at comparable stages (Bora *et al.*, 2021). Morphological observations of cell shrinkage, membrane blebbing, and detachment in S5-treated MCF-7 cells are consistent with CDK inhibition-mediated G1/S arrest and apoptosis, corroborating the proposed mechanism of action (Shanabag *et al.*, 2025; Hong *et al.*, 2024). Optimisation of the spiropyran scaffold through targeted structural modifications guided by SAR findings from the current study is expected to yield derivatives with improved potency in subsequent rounds of development.

From a drug-likeness perspective, S5 complied with all Lipinski Rule of Five criteria with no violations, demonstrating a favourable pharmacokinetic profile with acceptable TPSA (114.14 Å²) and rotatable bonds (7). This favourable drug-likeness pertains to physicochemical parameters and does not extend to the predicted toxicity profile, as S5, in common with the series, returned active predictions across several toxicity endpoints and a predicted LD_{50} (571.2 mg/kg) in the lower range of the series, underscoring the need for experimental genotoxicity and safety evaluation. The low predicted gastrointestinal absorption identified for all derivatives represents the primary formulation challenge for this series. Prodrug strategies or nanoparticle-based delivery platforms represent viable approaches to overcome this limitation, an avenue that warrants systematic investigation in future work (Adon *et al.*, 2021). The photoswitchable nature of the spiropyran scaffold presents an additional opportunity for spatiotemporally controlled drug activation in tumour tissue, a concept with growing precedent in oncology drug delivery (Fagan *et al.*, 2021).

Several limitations of the present study warrant acknowledgement. First, cytotoxicity was evaluated against a single breast cancer cell line (MCF-7), and generalisation of findings to other breast

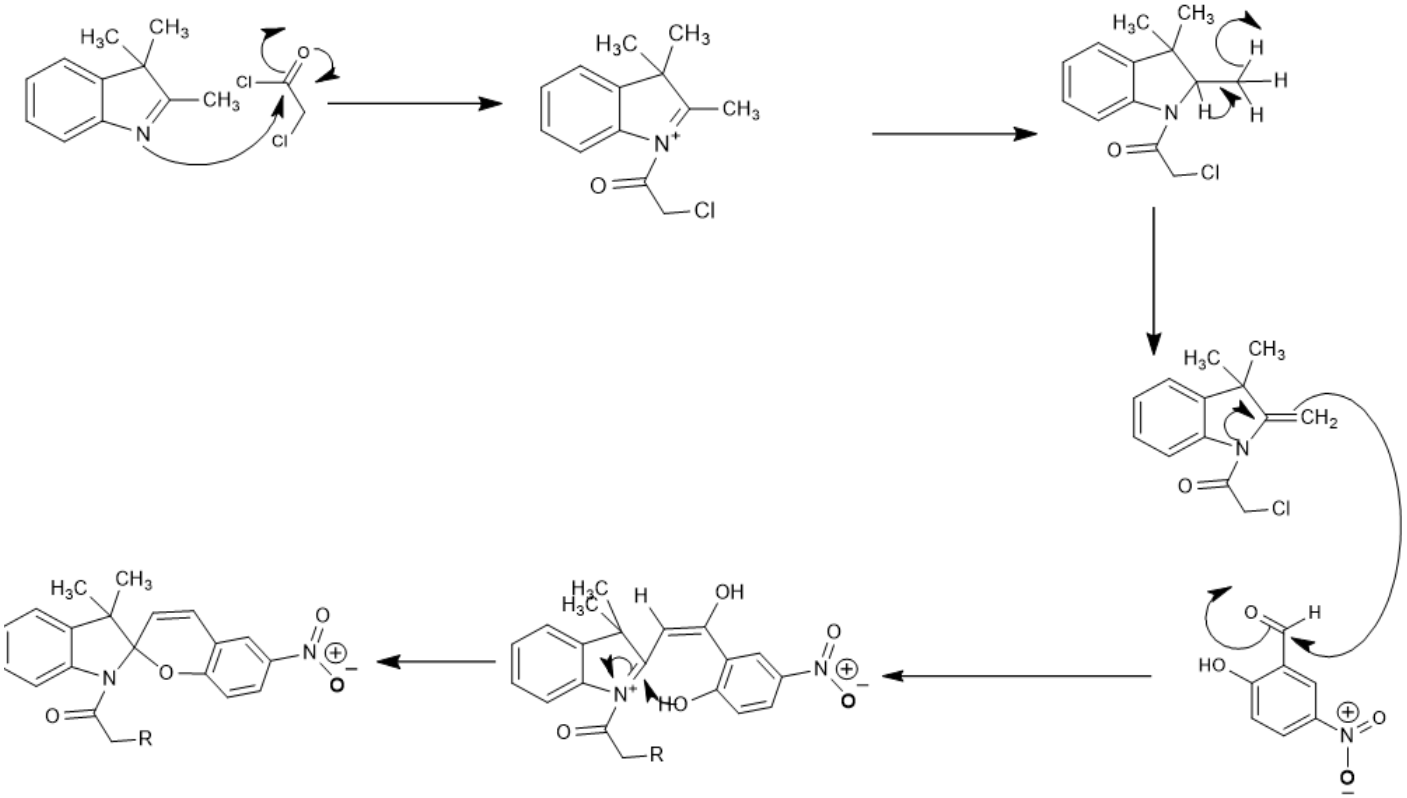


Figure 2: Proposed reaction mechanism for the synthesis of spiropyran derivatives.

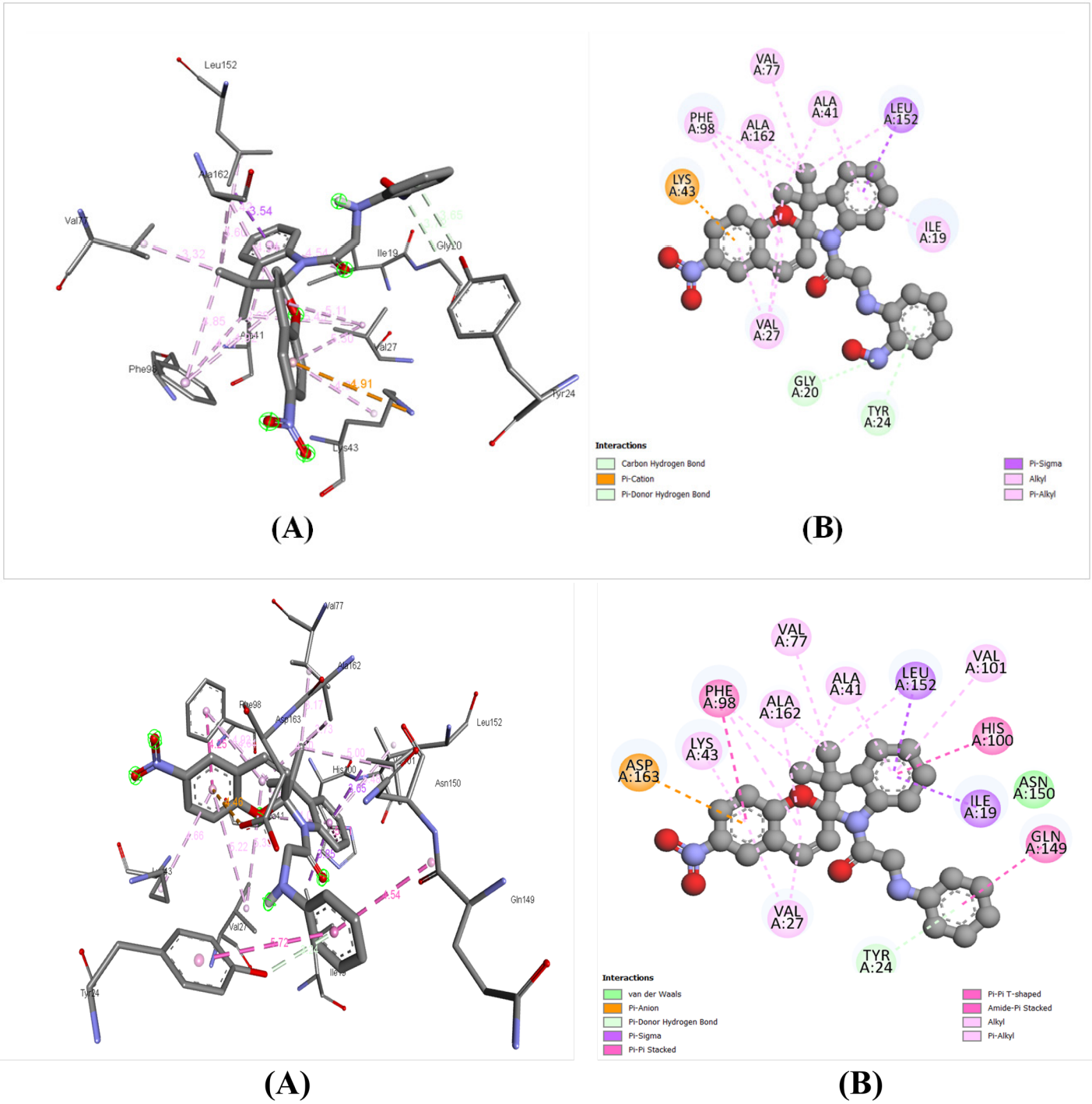


Figure 3: Molecular docking interactions with CDK6 (PDB ID: 5L2I). (A) 3D and 2D interaction diagrams for compound S5 (binding energy: -9.8 kcal/mol), showing hydrogen bonds with GLY20 and TYR24, and electrostatic interaction with LYS43. (B) Corresponding diagrams for compound S2 (binding energy: -9.1 kcal/mol). (C) Reference compound palbociclib (binding energy: -9.4 kcal/mol), showing hydrogen bonds with VAL101 and GLU99. Generated using BIOVIA Discovery Studio Visualizer v4.5.

cancer subtypes requires additional evaluation across a panel of cell lines. Second, CDK4 versus CDK6 isoform selectivity was not confirmed by experimental kinase profiling assays; the selectivity evidence remains computational, and *in vitro* kinase inhibition assays against both CDK4/Cyclin D1 and CDK6/Cyclin D3 are essential to substantiate selectivity claims. Third, *in vivo* pharmacokinetic and efficacy data are absent, and the compound's stability and tolerability require evaluation in appropriate animal models. Finally, the toxicity predictions were based on computational tools, and definitive safety profiling through standard preclinical genotoxicity and regulatory toxicology studies is required. The strengths of this study include

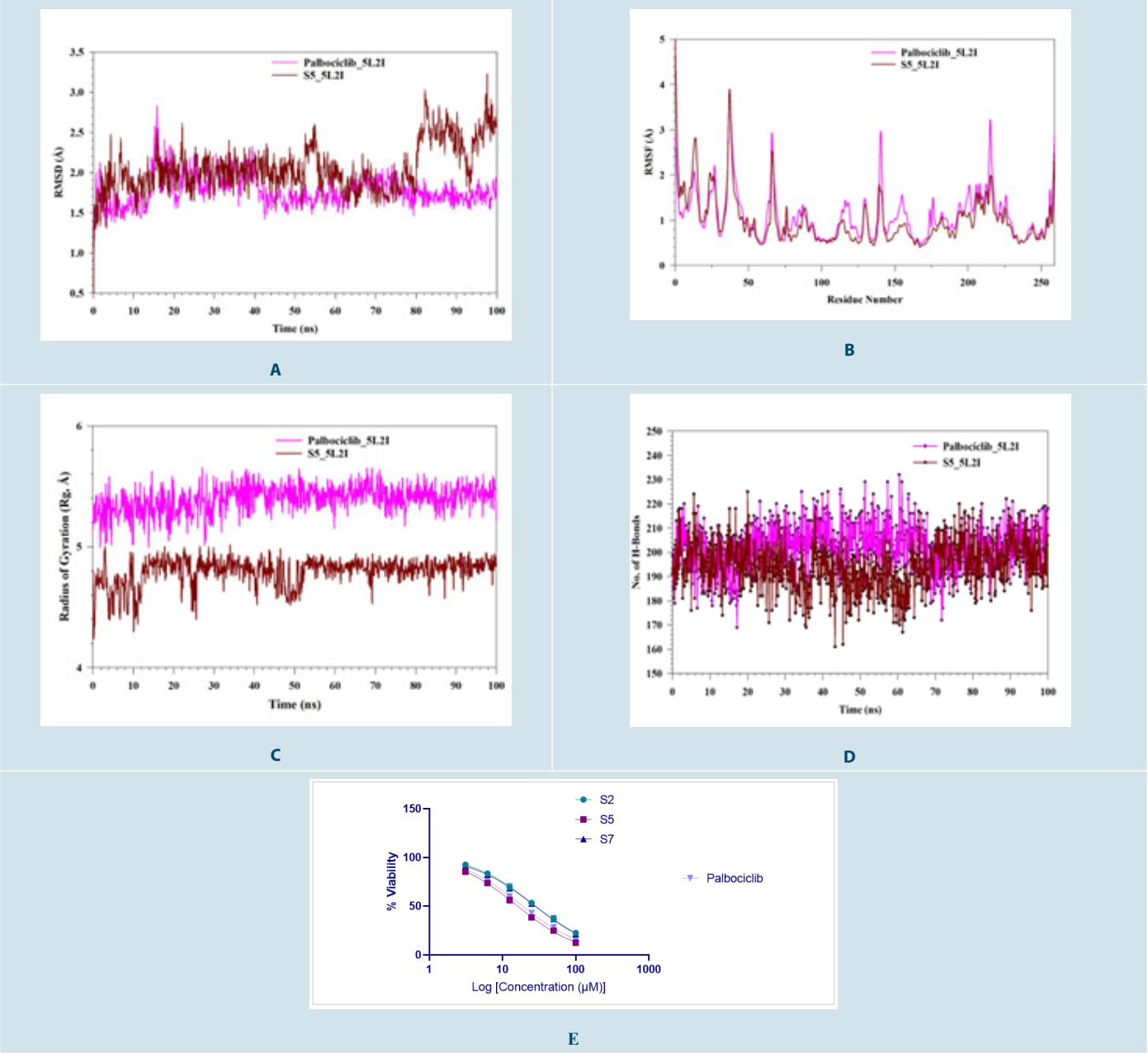


Figure 4: MD simulation analysis of 100 ns trajectories for palbociclib-CDK6 (pink) and S5-CDK6 (dark red) complexes, and *in vitro* cytotoxicity data. (A) RMSD of Cα backbone; (B) RMSF of Cα backbone; (C) Radius of gyration (Rg) of Cα backbone; (D) Hydrogen bond formation frequency; (E) Concentration-dependent cytotoxic effects of S5, S7, S2, and palbociclib on MCF-7 cells assessed by MTT assay (72 hr; Mean ± SD, *n*=3 independent experiments).

the multi-modal integrated approach combining rational design, *in silico* profiling, synthesis, and *in vitro* validation, the use of a validated docking platform cross-checked against AutoDock Vina, and the inclusion of 100 ns MD simulations providing robust dynamic assessment of CDK6 engagement. These findings establish spiropyran derivative S5 as a promising lead warranting advancement to comprehensive *in vivo* efficacy studies, kinase selectivity profiling, and structural optimisation campaigns.

CONCLUSION

This study presents the design, synthesis, and biological evaluation of novel spiropyran derivatives (S1-S8) as putative CDK6-targeting anticancer agents for breast cancer treatment. Compound S5 emerged as the lead candidate, exhibiting the highest predicted CDK6 docking affinity (-9.8 kcal/mol) in the series and cytotoxic potency (IC_{50}=15.58±1.24 μM) comparable to palbociclib against MCF-7 cells, while complying with all Lipinski Rule of Five criteria. Molecular docking and 100 ns MD simulations indicated stable CDK6 engagement through distinct binding interactions involving GLY20, TYR24, and LYS43, with

MM-GBSA analysis indicating a more favourable predicted binding free energy for S5 relative to palbociclib. Given that only three compounds were evaluated experimentally and that no kinase inhibition assays or quantitative correlation analyses were performed, these findings support preliminary agreement between computational and biological data rather than validation of the spiropyran scaffold for CDK6 inhibitor development. They nonetheless identify the spiropyran scaffold as a candidate framework worth further investigation, warranting direct CDK4 and CDK6 kinase inhibition and selectivity assays, evaluation across additional breast cancer and normal cell lines, *in vivo* efficacy studies, and structural optimisation before the series can be advanced toward preclinical development.

ACKNOWLEDGEMENT

The authors acknowledge Sciquaint Innovations Private Limited, Pune, India, for providing computational chemistry platforms (ForceADME, Geintox-II, GeinDock Suite) and supplying chemical reagents and reference standards. The National Centre for Cell Science (NCCS), Pune, India, is acknowledged for providing the MCF-7 cell line.

The authors thank Pravara Rural College of Pharmacy, Loni for providing the facility for research work.

ABBREVIATIONS

ADME: Absorption, Distribution, Metabolism, and Excretion; **BBB:** Blood-Brain Barrier; **CDK:** Cyclin-Dependent Kinase; **CI:** Confidence Interval; **DMEM:** Dulbecco's Modified Eagle Medium; **DMSO:** Dimethyl Sulfoxide; **ESI:** Electrospray Ionisation; **FBS:** Fetal Bovine Serum; **GI:** Gastrointestinal; **HBA:** Hydrogen Bond Acceptors; **HBD:** Hydrogen Bond Donors; **IC_{50}:** Half-maximal Inhibitory Concentration; **IR:** Infrared Spectroscopy; **LogP:** Logarithm of Partition Coefficient; **MD:** Molecular Dynamics; **MMFF94:** Merck Molecular Force Field 94; **MM-GBSA:** Molecular Mechanics Generalised Born Surface Area; **MTT:** 3-(4,5-dimethylthiazol-2-yl)-2,5-diphenyltetrazolium bromide; **MW:** Molecular Weight; **NCCS:** National Centre for Cell Science; **NMR:** Nuclear Magnetic Resonance; **PDB:** Protein Data Bank; **Rb:** Retinoblastoma protein; **RMSD:** Root Mean Square Deviation; **RMSF:** Root Mean Square Fluctuation; **Rg:** Radius of Gyration; **SASA:** Solvent Accessible Surface Area; **SD:** Standard Deviation; **TPSA:** Total Polar Surface Area.

CONFLICT OF INTEREST

The authors declare that there is no conflict of interest.

AUTHOR CONTRIBUTIONS

Sagar D. Magar: Conceptualisation, methodology, synthesis of derivatives, spectroscopic characterisation, data analysis, manuscript writing, review and editing. Shubham **P. Mankar and Sanket K. Tambe:** Synthesis of derivatives, spectroscopic characterisation. **Amol S. Dighe and Mayur S. Bhosale:** ADME and toxicity analysis, molecular docking studies, validation of computational studies. **Nilima M. Wani:** Data analysis, manuscript writing, review and editing. **Rahul K. Godge, Dattaprasad N. Vikhe and Jagdish R. Kudnar:** Manuscript review and editing.

REFERENCES

Adon, T., Shanmugarajan, D., & Kumar, H. Y. (2021). CDK4/6 inhibitors: A brief overview and prospective research directions. RSC Advances, 11(50), 29227-46. https://doi.org/10.1039/d1ra03820f

Ali, A. A., Kharbash, R., & Kim, Y. (2020). Chemo- and biosensing applications of spiropyran and its derivatives - A review. Analytica Chimica Acta, 1110, 199-223. https://doi.org/10.1016/j.aca.2020.01.057

Banerjee, P., Kemmler, E., Dunkel, M., & Preissner, R. (2024). ProTox 3.0: A webserver for the prediction of toxicity of chemicals. Nucleic Acids Research, 52(W1), W513-W520. https://doi.org/10.1093/nar/gkae303

Bhandari, S. V., Nagras, O. G., Patil, S. M., *et al.* (2026). Exploring ionic liquid-based methods in the synthesis of benzimidazole-1,3,4-oxadiazole derivatives for EGFR inhibition. Journal of Molecular Structure, 1351, 143981. https://doi.org/10.1016/j.molstruc.2025.143981

Bora, D., Kaushal, A., & Shankaraiah, N. (2021). Anticancer potential of spirocompounds in medicinal chemistry: A pentennial expedition. European Journal of Medicinal Chemistry, 215, 113263. https://doi.org/10.1016/j.ejmech.2021.113263

Bowers, K. J., Chow, E., Xu, H., *et al.* (2006). Scalable algorithms for molecular dynamics simulations on commodity clusters. In Proceedings of the 2006 ACM/IEEE Conference on Supercomputing (p. 84). ACM.

Dasmahapatra, U., Kumar, C. K., Das, S., *et al.* (2022). *In silico* molecular modelling, MM/GBSA binding free energy and molecular dynamics simulation study of novel pyrido fused imidazo [4,5-c] quinolines. Frontiers in Chemistry, 10. https://doi.org/10.3389/fchem.2022.991369

Debnath, A., Mazumder, R., Singh, A. K., & Singh, R. K. (2025). Identification of novel cyclin-dependent kinase 4/6 inhibitors from marine natural products. PLOS ONE, 20(1), e0313830. https://doi.org/10.1371/journal.pone.0313830

Durrant, J. D., & McCammon, J. A. (2011). Molecular dynamics simulations and drug discovery. BMC Biology, 9(1), 71. https://doi.org/10.1186/1741-7007-9-71

Ertl, P., Rohde, B., & Selzer, P. (2000). Fast calculation of molecular polar surface area as a sum of fragment-based contributions. Journal of Medicinal Chemistry, 43(20), 3714-3717. https://doi.org/10.1021/jm000942e

Fagan, A., Bartkowski, M., & Giordani, S. (2021). Spiropyran-based drug delivery systems. Frontiers in Chemistry, 9. https://doi.org/10.3389/fchem.2021.720087

Farhadi, B., Beygisangchin, M., Ghamari, N., *et al.* (2025). Molecular dynamics simulations of proteins: An in-depth review of computational strategies, structural insights, and their role in medicinal chemistry and drug development. Biological Cybernetics, 119(4), 28. https://doi.org/10.1007/s00422-025-01026-0

Forouzesh, N., & Mishra, N. (2021). An effective MM/GBSA protocol for absolute binding free energy calculations. Molecules, 26(8), 2383. https://doi.org/10.3390/molecules26082383

Ghasemi, M., Turnbull, T., Sebastian, S., & Kempson, I. (2021). The MTT assay: Utility, limitations, pitfalls, and interpretation. International Journal of Molecular Sciences, 22(23), 12827. https://doi.org/10.3390/ijms222312827

Grewal, S., Deswal, G., Grewal, A. S., & Guarve, K. (2025). Molecular dynamics simulations: Insights into protein and protein ligand interactions. Advances in Pharmacology, 103, 139-162. https://doi.org/10.1016/bs.apha.2025.01.007

Hong, T., Hogger, A. C., Wang, D., *et al.* (2024). CDK4/6 inhibition initiates cell cycle arrest by nuclear translocation of RB and induces a multistep molecular response. Cell Death Discovery, 10(1), 453. https://doi.org/10.1038/s41420-024-02218-6

Hughes-Whiffing, C. A., & Perry, A. (2023). Three complementary one-pot four-component reaction sequences for rapid, general and direct spiropyran synthesis. European Journal of Organic Chemistry, 26(2), e202201245. https://doi.org/10.1002/ejoc.202201245

Ivanova, L., Tammiku-Taul, J., Garcia-Sosa, A. T., *et al.* (2018). Molecular dynamics simulations of the interactions between glial cell line-derived neurotrophic factor family receptor GFRα1 and small-molecule ligands. ACS Omega, 3(9), 11407-11414. https://doi.org/10.1021/acsomega.8b01524

Ji, W., Zhang, W., Wang, X., *et al.* (2020). c-myc regulates the sensitivity of breast cancer cells to palbociclib via c-myc/miR-29b-3p/CDK6 axis. Cell Death & Disease, 11(9), 760. https://doi.org/10.1038/s41419-020-02980-2

Keyvan Rad, J., Balzade, Z., & Mahdavian, A. R. (2022). Spiropyran-based advanced photoswitchable materials: A fascinating pathway to the future stimuli-responsive devices. Journal of Photochemistry and Photobiology C, 51, 100487. https://doi.org/10.1016/j.jphotochemrev.2022.100487

Kim, S., Leong, A., Kim, M., & Yang, H. W. (2022). CDK4/6 initiates Rb inactivation and CDK2 activity coordinates cell-cycle commitment and G1/S transition. Scientific Reports, 12(1), 16810. https://doi.org/10.1038/s41598-022-20769-5

Li, L., Liu, S., Wang, B., *et al.* (2023). An updated review on developing small molecule kinase inhibitors using computer-aided drug design approaches. International Journal of Molecular Sciences, 24(18), 13953. https://doi.org/10.3390/ijms241813953

Lipinski, C. A. (2004). Lead- and drug-like compounds: The rule-of-five revolution. Drug Discovery Today: Technologies, 1(4), 337-341. https://doi.org/10.1016/j.ddtec.2004.11.007

Loibl, S., & Furlanetto, J. (2022). Integrating CDK4/6 inhibitors in the treatment of patients with early breast cancer. The Breast, 62, S70-S79. https://doi.org/10.1016/j.breast.2021.12.008

Luo, X., Zhao, Y., Tang, P., *et al.* (2021). Discovery of new small-molecule cyclin-dependent kinase 6 inhibitors through computational approaches. Molecular Diversity, 25(1), 367-382. https://doi.org/10.1007/s11030-020-10120-3

Mandal, M., Banik, D., Karak, A., *et al.* (2022). Spiropyran-merocyanine based photochromic fluorescent probes: Design, synthesis, and applications. ACS Omega, 7(41), 36988-37007. https://doi.org/10.1021/acsomega.2c04969

Manzoor, H., Khan, M. U., Rehman, R., *et al.* (2025). Identification and evaluation of pyrimidine based CDK6 inhibitors against glioblastoma using integrated computational approaches. Scientific Reports, 15(1), 25387. https://doi.org/10.1038/s41598-025-10744-1

Martin, M. P., Endicott, J. A., & Noble, M. E. M. (2017). Structure-based discovery and development of cyclin-dependent protein kinase inhibitors. Essays in Biochemistry, 61(5), 439-452. https://doi.org/10.1042/EBC20170040

Piezzo, M., Chiodini, P., Riemma, M., *et al.* (2020). Progression-free survival and overall survival of CDK 4/6 inhibitors plus endocrine therapy in metastatic breast cancer: A systematic review and meta-analysis. International Journal of Molecular Sciences, 21(17), 6400. https://doi.org/10.3390/ijms21176400

Rana, S., Bendjennat, M., Kour, S., *et al.* (2019). Selective degradation of CDK6 by a palbociclib based PROTAC. Bioorganic & Medicinal Chemistry Letters, 29(11), 1375-1379. https://doi.org/10.1016/j.bmcl.2019.03.035

Ramazi, S., Salimian, M., Allahverdi, A., *et al*. (2023). Synergistic cytotoxic effects of an extremely low-frequency electromagnetic field with doxorubicin on MCF-7 cell line. Scientific Reports, 13(1), 8844. https://doi.org/10.1038/s41598-023-35767-4

Razak, N. A., Abu, N., Ho, W. Y., *et al*. (2019). Cytotoxicity of eupatorin in MCF-7 and MDA-MB-231 human breast cancer cells via cell cycle arrest, anti-angiogenesis and induction of apoptosis. Scientific Reports, 9(1), 1514. https://doi.org/10.1038/s41598-018-37796-w

Sarac, B., Yücer, S., Ciftci, F., *et al.* (2025). Molecular dynamics simulations and their novel applications in drug delivery for cancer treatment: A review. Annals of Biomedical Engineering, 53(12), 3254-3284. https://doi.org/10.1007/s10439-025-03864-2

Scheicher, R., Hoelbl-Kovacic, A., Bellutti, F., *et al*. (2015). CDK6 as a key regulator of hematopoietic and leukemic stem cell activation. Blood, 125(1), 90-101. https://doi.org/10.1182/blood-2014-06-584417

Schettini, F., Giudici, F., Giuliano, M., *et al*. (2020). Overall survival of CDK4/6-inhibitor-based treatments in clinically relevant subgroups of metastatic breast cancer: Systematic review and meta-analysis. Journal of the National Cancer Institute, 112(11), 1089-1097. https://doi.org/10.1093/jnci/djaa071

Shanabag, A., Armand, J., Son, E., & Yang, H. W. (2025). Targeting CDK4/6 in breast cancer. Experimental & Molecular Medicine, 57(2), 312-322. https://doi.org/10.1038/s12276-025-01395-3

Sherr, C. J., Beach, D., & Shapiro, G. I. (2016). Targeting CDK4 and CDK6: From discovery to therapy. Cancer Discovery, 6(4), 353-367. https://doi.org/10.1158/2159-8290.CD-15-0894

Shivakumar, D., Williams, J., Wu, Y., *et al*. (2010). Prediction of absolute solvation free energies using molecular dynamics free energy perturbation and the OPLS force field. Journal of Chemical Theory and Computation, 6(5), 1509-1519. https://doi.org/10.1021/ct900587b

Stanciu, I. M., Parosanu, A. I., & Nitipir, C. (2023). An overview of the safety profile and clinical impact of CDK4/6 inhibitors in breast cancer: A systematic review of randomized phase II and III clinical trials. Biomolecules, 13(9), 1422. https://doi.org/10.3390/biom13091422

Susanti, N. M. P., Damayanti, S., Kartasasmita, R. E., & Tjahjono, D. H. (2021). A search for cyclin-dependent kinase 4/6 inhibitors by pharmacophore-based virtual screening, molecular docking, and molecular dynamic simulations. International Journal of Molecular Sciences, 22(24), 13423. https://doi.org/10.3390/ijms222413423

Tadesse, S., Yu, M., Kumarasiri, M., *et al*. (2015). Targeting CDK6 in cancer: State of the art and new insights. Cell Cycle, 14(20), 3220-3230. https://doi.org/10.1080/15384101.2015.1084445

Topacio, B. R., Zatulovskiy, E., Cristea, S., *et al*. (2019). Cyclin D-Cdk4,6 drives cell-cycle progression via the retinoblastoma protein's C-terminal helix. Molecular Cell, 74(4), 758-770.e4. https://doi.org/10.1016/j.molcel.2019.03.020

Wander, S. A., O'Brien, N., Litchfield, L. M., *et al.* (2022). Targeting CDK4 and 6 in cancer therapy: Emerging preclinical insights related to abemaciclib. The Oncologist, 27(10), 811-821. https://doi.org/10.1093/oncolo/oyac138

Watt, A. C., & Goel, S. (2022). Cellular mechanisms underlying response and resistance to CDK4/6 inhibitors in the treatment of hormone receptor-positive breast cancer. Breast Cancer Research, 24(1), 17. https://doi.org/10.1186/s13058-022-01510-6

Wells, C. I., Vasta, J. D., Corona, C. R., *et al*. (2020). Quantifying CDK inhibitor selectivity in live cells. Nature Communications, 11(1), 2743. https://doi.org/10.1038/s41467-020-16559-0

Zhou, F. H., Downton, T., Freelander, A., *et al*. (2023). CDK4/6 inhibitor resistance in estrogen receptor positive breast cancer, a 2023 perspective. Frontiers in Cell and Developmental Biology, 11, 1148792. https://doi.org/10.3389/fcell.2023.1148792

Cite this article: Magar SD, Mankar SP, Tambe SK, Dighe AS, Wani NM, Bhosale MS, *et al*. Design, Synthesis and Molecular Dynamics Simulation of Novel Spiropyran Derivatives as Putative CDK6-Targeting Anticancer Agents for Breast Cancer Treatment. J Young Pharm. 2026;18(3):709-19.